Ocean Dynamics (2022) 72:405–419
https://doi.org/10.1007/s10236-022-01506-y

Propagation of barotropic Kelvin waves around Antarctica

David J. Webb[1] · Ryan M. Holmes[2,3] · Paul Spence[4] · Matthew H. England[5]

Received: 24 February 2022 / Accepted: 10 March 2022 / Published online: 5 May 2022

Abstract

Barotropic (i.e., depth-uniform) coastal oceanic Kelvin waves can provide rapid teleconnections from climate and weather events in one location to remote regions of the globe. Studies suggest that barotropic Kelvin waves observed around Antarctica may provide a mechanism for rapidly propagating circulation anomalies around the continent, with implications for continental shelf temperatures along the West Antarctic Peninsula and thus Antarctic ice mass loss rates. However, how the propagation of Kelvin waves around Antarctica is influenced by features such as coastal geometry and variations in bathymetry remains poorly understood. Here we study the propagation of barotropic Antarctic Kelvin waves using a range of idealized model simulations. Using a single-layer linear shallow water model with 1° horizontal resolution, we gradually add complexity of continental configuration, realistic bathymetry, variable planetary rotation, and forcing scenarios, to isolate sources and sinks of wave energy and the mechanisms responsible. We find that approximately 75% of sub-inertial barotropic Kelvin wave energy is scattered away from Antarctica as other waves in one circumnavigation of the continent, due mostly to interactions with bathymetry. Super-inertial barotropic Kelvin waves lose nearly 95% of their energy in one circumpolar loop, due to interactions with both coastal geometry and bathymetry. These results help to explain why only sustained signals of low-frequency resonant barotropic Kelvin waves have been observed around Antarctica, and contribute to our understanding of the role of rapid, oceanic teleconnections in climate.

Keywords Barotropic Kelvin waves · Planetary waves · Wave propagation · Antarctica

Responsible Editor: Richard John Greatbatch

✉ Ryan M. Holmes
r.holmes@sydney.edu.au

1 ARC Centre of Excellence for Climate System Science, Climate Change Research Centre, University of New South Wales, Sydney, Australia

2 ARC Centre of Excellence for Climate Extremes, Climate Change Research Centre and the School of Mathematics and Statistics, University of New South Wales, Sydney, Australia

3 School of Geosciences, University of Sydney, Sydney, NSW, Australia

4 The Australian Centre for Excellence in Antarctic Science, Institute for Marine and Antarctic Studies and the Australian Antarctic Partnership Program, University of Tasmania, Hobart, Australia

5 The Australian Centre for Excellence in Antarctic Science and Climate Change Research Centre, University of New South Wales, Sydney, Australia

1 Introduction

The ocean admits a rich variety of wave-like motions which play a key role in its dynamics. Horizontally propagating planetary-scale oceanic waves such as Kelvin, Rossby, and Poincaré waves transmit information rapidly from one location to another and lie at the core of many mechanistic explanations for climatic modes of variability (e.g., the El Niño-Southern Oscillation). The focus of this study is on barotropic (depth-uniform) waves, which have rapid propagation speeds and large deformation radii (approximately 200 m/s and 1500 km respectively for an ocean of depth 4000m at 60° latitude, e.g., Rhines 1969). While in the presence of topographic slopes the separation of barotropic and baroclinic modes is not strictly possible (Garrett 1978; Fu et al. 1982; Pickart 1995; LaCasce 2017), barotropic wave dynamics has provided useful insights into a variety of oceanic phenomenon. For example, tidally induced and storm-generated barotropic waves have been

shown to influence shallow sea and shelf regions (e.g., Simionato et al. 2005; Mercer et al. 2002) and provide a mechanism for rapid basin-wide adjustment (Jayne and Marotzke 2001; Spence et al. 2017; Webb et al. 2019). Coastal trapped barotropic waves also influence coastal upwelling with implications for biological productivity (e.g., Pietri et al. 2014; Huthnance 1980).

This study will focus on barotropic coastal-trapped Kelvin waves around Antarctica. The circumpolar Antarctic continent provides a periodic waveguide for Kelvin waves that permits resonance at a set of quantized frequencies (Platzman et al. 1981; Zahel and Müller 2005). By fitting sea level observations to these resonance conditions, Kusahara and Ohshima (2014) identify statistically significant signals corresponding to the first three circumpolar modes, with periods of approximately 32, 16, and 11 h, respectively. Using bottom pressure data, Ponte and Hirose (2004) also provide some evidence for circumpolar propagating signals with similar frequencies, although they suggest that strong frictional dissipation may make their global signal more difficult to detect. More recently, model studies have suggested that barotropic Kelvin waves may play an important role in facilitating subsurface warming along the West Antarctic Peninsula under future climate scenarios (Spence et al. 2017; Webb et al. 2019), with implications for Antarctic ice sheet mass loss (Schmidtko et al. 2014; Rignot et al. 2002). Spence et al. (2017) proposed that barotropic Kelvin waves generated by localized wind perturbations in East Antarctica could lead to the development of rapid barotropic velocity anomalies around the entire continent. These barotropic velocity anomalies, amplified in regions of strong f/H gradients such as the West Antarctic Peninsula, impact the bottom stress leading to bottom Ekman transport anomalies that drive warm Circumpolar Deep Water onto the Antarctic shelf. Webb et al. (2019) quantify the potential bottom Ekman transport anomalies and its sensitivity to the background state, suggesting that this mechanism could lead to warming of up to 0.7°C along the Antarctic Peninsula within a year under wind forcing anomalies typical of the recent trends in the Southern Annular Mode (SAM). The key hypothesized role of barotropic Kelvin waves in this adjustment process highlight the need for a better understanding of barotropic wave dynamics around Antarctica, in particular those processes that influence the scattering and/or intensification of Kelvin wave energy. This is the goal of the present study.

Barotropic Kelvin waves can be generated by a variety of sources including wind stress anomalies associated with storms, flow over bathymetry and interactions with other waves (e.g., tides). In turn, Kelvin waves encountering bathymetric features or changes in coastal geometry can scatter into other wave types, ultimately leading to a loss of barotropic Kelvin wave energy in the Antarctic waveguide. Broadly speaking, these other wave types include planetary and topographic Rossby waves associated with gradients in the Coriolis parameter f and bathymetry H, respectively, Poincaré waves, and other dispersive coastally trapped waves (e.g., Mysak 1980; Brink 1991; Wilkin and Chapman 1990), although in the presence of complex bathymetry, strictly speaking no such clean delineation exists (Huthnance 1978; 1980). The dynamics of these wave scattering interactions are complex. Even in linear flat bottom models that do permit an exact Kelvin wave solution, many interesting phenomenon arise. Packham and Williams (1968) showed that the transmission of barotropic Kelvin waves around an angle in the coastline depends on frequency, in a quantized manner, with the remaining energy lost to Poincaré waves. Buchwald and Miles (1974) studied barotropic Kelvin waves diffracting due to a gap in the coastline and showed that Kelvin waves can "jump" across coastal gaps that are sufficiently small compared to the deformation radius, highlighting the potential for barotropic Kelvin waves to cross Drake Passage (approximately 1000-km wide) and communicate with the Pacific, Indian, and Atlantic basins. This highlights the potential for these waves to play an important role in climate through high- to mid-latitude oceanic teleconnections along with other, baroclinic, oceanic wave teleconnection mechanisms (e.g., McDermott 1996; Johnson and Marshall 2002; Brix and Gerdes 2003; Ivchenko et al. 2004; Atkinson et al. 2009; Blaker et al. 2006; Webb et al. 2021).

Ocean tides also propagate as barotropic waves and can influence the energetics of the Antarctic circulation. Recent studies suggest that tides may play an important role in the Antarctic shelf heat budget (Stewart et al. 2018; Lianillo 2013), as well as directly influencing the ice shelf (e.g., Rosier et al. 2014). Tides also drive strong dissipation and mixing through interactions with topographic features and stratification. However, the focus of this study is on the propagation of the barotropic Kelvin waves that are most likely to sustain a signal around Antarctica, i.e., those obeying resonance conditions around the continent (Platzman et al. 1981; Kusahara and Ohshima 2014). These frequencies do not correspond to tidal frequencies.

In this study, we estimate the energy distribution and energy flux of barotropic Kelvin waves propagating around Antarctica using a global shallow-water model. Unlike previous modeling studies (e.g., Platzman et al. 1981; Zahel and Müller 2005), we start with a flat-bottom, linear coastline, f-plane single-layer shallow water model and systematically introduce variations in bathymetry, Coriolis parameter, and coastal geometry in order to determine the dominant processes responsible for scattering barotropic Kelvin waves out of the Antarctic waveguide. It is important to note that the frictional processes acting on barotropic Kelvin waves around Antarctica are somewhat uncertain

and unconstrained in observations (Ponte and Hirose 2004). We do not address this issue in detail here. Rather, we focus our study on the influence of these waves in widely used global ocean climate models, where they have been shown to influence oceanic properties along the Antarctic continental shelf (e.g., Webb et al. 2019). The rest of the paper is divided as follows: in Section 2, we present the background theory for waves produced in a linearized single-layer ocean model and their corresponding energy fluxes. Section 3 discusses the models and the parameters that are varied. Section 4 presents our model results, and finally Section 5 provides a discussion and summarizes our conclusions.

2 Background theory and methodology

In this section, we provide an overview of shallow water wave theory, describing the various wave-types that barotropic Kelvin waves can lose energy to. The linearized single-layer shallow water equations with no mean flow in the presence of bottom friction (and a variable bottom depth) are given by

$$\frac{\partial u}{\partial t} - fv = -g\frac{\partial \eta}{\partial x} + \tau_x \tag{1}$$

$$\frac{\partial v}{\partial t} + fu = -g\frac{\partial \eta}{\partial y} + \tau_y \tag{2}$$

$$\frac{\partial \eta}{\partial t} + \frac{\partial}{\partial x}(Hu) + \frac{\partial}{\partial y}(Hv) = 0, \tag{3}$$

where f is the Coriolis parameter, H is depth, ρ_0 represents the single-layer fluid density, g is the gravitational constant, u and v are the zonal and meridional velocity components, η is the displacement in sea surface height, and τ_x and τ_y are the zonal and meridional components of bottom-stress, respectively. We assume a linearized model with no mean flow, which is appropriate for barotropic waves whose rapid phase speed of $O(100ms^{-1})$ is two orders of magnitude larger than typical mean flow speeds, $O(1ms^{-1})$. Combining Eqs. 1–3 leads to an expression for the total energy density, $E(Jm^{-2})$, which is the sum of kinetic and potential contributions,

$$E = \frac{1}{2}\rho_0 H\mathbf{u}^2 + \frac{1}{2}\rho_0 g\eta^2, \tag{4}$$

where $\mathbf{u} = (u, v)$. The associated energy flux vector (Wm^{-1}) is given by,

$$\mathbf{F} = \mathbf{u}\rho_0 gH\eta, \tag{5}$$

satisfying conservation of energy in the presence of bottom friction, $\boldsymbol{\tau}_B = (\tau_x, \tau_y)$, and a variable bottom depth, i.e.,

$$\frac{\partial E}{\partial t} + \nabla \cdot \mathbf{F} = \rho_0 H\left(\boldsymbol{u} \cdot \boldsymbol{\tau}_B\right). \tag{6}$$

Equation 6 holds for all of our single-layer model runs and measures the combined energy flux (and energy density) of all wave-types present in the model. By comparing the energy fluxes across a range of idealized experiments, we determine the amount of scattering of Kelvin wave energy out of the Antarctic waveguide due to various factors discussed below including changes in coastal geometry, bathymetry, Coriolis parameter, and the presence or absence of the South American continent that permits Kelvin wave energy to cross Drake Passage.

2.1 Changes in coastal geometry

For a flat bottom on an f-plane with Coriolis parameter f_0, wave solutions to Eqs. 1–3 are known as Poincaré waves and obey the dispersion relation

$$\omega^2 = f_0^2 + gH(k^2 + l^2), \tag{7}$$

where ω is the frequency and k and l are the zonal and meridional wavenumbers. Although Poincaré waves are typically generated by wind forcing, they can also be radiated by Kelvin waves propagating along a jagged coastline. The amount of energy scattered into Poincaré waves is determined by the Kelvin wave frequency and the geometry of the coastline. Packham and Williams (1968) showed that there exist critical angles,

$$\theta_n = \frac{\pi}{2n+1}, \tag{8}$$

for any positive integer, n, along an idealized coastline with only one angle change, for which no Poincaré waves are generated. These angles are independent of frequency indicating all propagating Kelvin waves travel unimpeded around such angles. In addition, oscillatory Poincaré waves only exist for frequencies greater than the inertial frequency (i.e., super-inertial frequencies, $\omega > f_0$, Eq. 7). This implies that Kelvin waves below the inertial frequency (i.e., sub-inertial frequencies, $\omega < f_0$) cannot generate propagating Poincaré waves that are able to radiate energy a significant distance away from the coastline (although we note that evanescent Poincarè waves can play a role in channels and straits, e.g., Taylor 1922).

2.2 Changes in rotation and bathymetry

When variations in f and/or H are introduced, a variety of other wave types are permitted. For flat bathymetry on a β-plane, $f = f_0 + \beta y$, planetary Rossby waves emerge obeying the dispersion relation,

$$\omega = -\beta\frac{k}{L_r^{-2} + k^2 + l^2}, \tag{9}$$

where $L_r = \sqrt{gH}/f_0$ is the radius of deformation and the zonal and meridional wave numbers are represented by

k and l respectively. These waves can serve as a sink for barotropic Kelvin waves, but only at low-frequencies below the maximum Rossby wave frequency of $\beta L_d/2$, which correspond to a period of $\sim$ 8 days for a 4000-m-deep ocean at 60°S (below the resonant frequencies for Antarctic barotropic Kelvin waves, Kusahara and Ohshima 2014).

When variations in bathymetry are also introduced a variety of other wave types emerge, depending on the particular bathymetry configuration. For simple linear slopes away from a coastline, these waves are generally known as topographic Rossby waves and obey a similar dispersion relation as Eq. 9. However, for more complex bathymetry such as the Antarctic shelf-slope, a strict separation between these different wave types gives way to a broad continuum of various types of dispersive coastally trapped slope and shelf waves (e.g., Mysak 1980; Brink 1991; Wilkin and Chapman 1990; McKee and Martinson 2020). While in this situation the barotropic Kelvin wave ceases to exist as an exact solution, in reality, a similar mode exists due to the scale separation between the barotropic deformation radius and the slope-shelf bathymetry. However, these additional bathymetric waves can still serve as a sink for barotropic Kelvin wave energy, which we examine below by comparing model simulations with and without bathymetry.

2.3 Drake Passage "jumping"

Idealized studies have shown that Kelvin waves can cross gaps in the coast such as bays, providing that the gap is comparable or smaller than the deformation radius (Buchwald and Miles 1974). This property allows a component of barotropic Kelvin waves propagating around Antarctica to cross Drake Passage and continue propagating northward along the east coast of South America. Conversely, Kelvin waves propagating southward along South America's west coast can transfer a component of their energy to Antarctica where it will continue to propagate westward around Antarctica's coastline. It is also worth mentioning that the first baroclinic Kelvin wave mode has a deformation radius of order 10km in the Southern Ocean (compared to approximately 1000km across Drake Passage) so only barotropic Kelvin waves have the ability to jump across Drake Passage.

3 Model descriptions and experimental design

3.1 Single-layer model

We use a single-layer, global shallow water model, based on a single-layer version of the Regional Ocean Modeling System (ROMS, Shchepetkin and McWilliams 2005), at 1° horizontal resolution (suitable for resolving barotropic waves). We use a 10-s time-step, sufficient to temporally resolve the highest frequency barotropic Kelvin waves we consider. Consistent with Eqs. 1–3, the non-linear advection terms are not included and we do not include any explicit horizontal viscosity. We use quadratic bottom drag with a coefficient of 1×10^{-3}. While bottom drag coefficients are uncertain, we found little sensitivity to the bottom drag coefficient for values smaller than this, although we expect that larger coefficients would lead to attenuation of the Kelvin wave signal and thus reduced circumpolar propagation. Boundary and forcing conditions are set according to the individual experiments described below.

3.2 Experimental design

In order to estimate the amount of energy lost in a single circumnavigation around Antarctica, the first series of experiments we consider use a non-reentrant domain, both with bathymetry (variable sea-floor depth) and without bathymetry (flat sea-floor). We force Kelvin waves from the eastern boundary (i.e., at 0°W) and apply radiation conditions (Flather 1976; Chapman 1985) on the eastern and western boundaries. The Kelvin wave is forced at the eastern boundary by applying the theoretical Kelvin wave solution for sea-surface height and zonal velocity in a flat bottom ocean, where we assume an ocean depth of 4000m.

In an additional set of experiments, designed to examine resonance and the long-term energy propagation of barotropic Kelvin waves around Antarctica, we instead apply re-entrant zonal boundary conditions and force the Kelvin waves using a time-variant wind stress (approximately $0.1 N/m^2$ applied between 20°E and 120°E, see Fig. 1). The spatial distribution of this wind forcing scenario is motivated by recent trends towards a positive phase of the Southern Annular Mode and is chosen to remain consistent with studies attributing Antarctic coastal circulation changes to barotropic Kelvin waves (Spence et al. 2017; Webb et al. 2019).

Barotropic Kelvin waves around Antarctica have been observed for periods corresponding to the first three resonant frequencies, ω_n, around Antarctica (Kusahara and Ohshima 2014). That is, for n=1,2,3, satisfying

$$n\frac{\sqrt{gH}}{\omega_n} = 2\pi r \tag{10}$$

where r is the average radial distance from the South Pole to the Antarctic coastline, and H is the average ocean depth over the barotropic waveguide (Platzman et al. 1981). For this reason, we focus on the first four resonant frequencies; the three observed barotropic Kelvin waves and the next

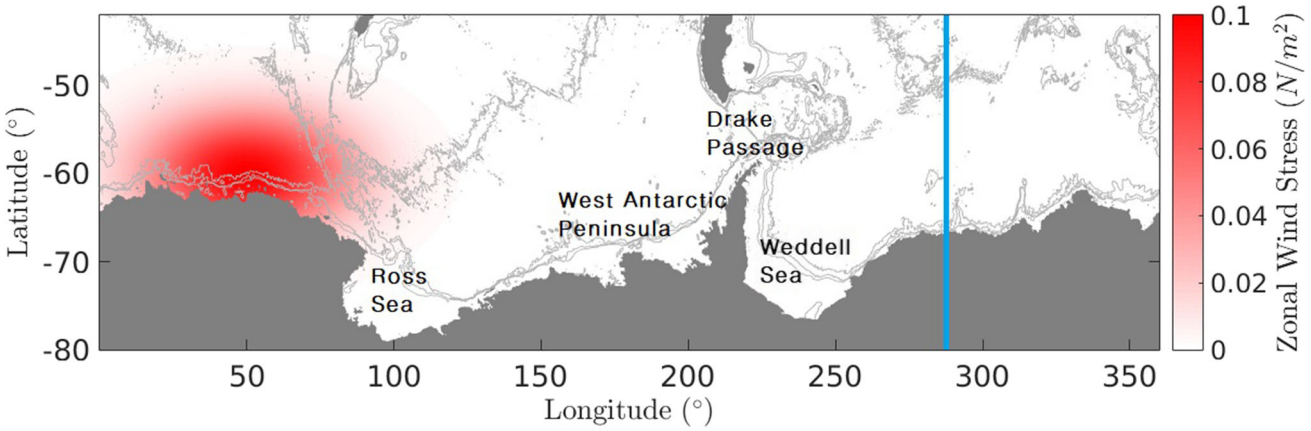

Fig. 1 Southern Ocean section indicating geographic regions of interest with maximum zonal wind stress (N/m^2) used in the 1- and 2-layer wind-forced experiments. The blue line indicates the location of the eastern boundary in the 1° single-layer boundary forced experiments and the thin gray lines represent the 1000-m, 2000-m, and 3000-m bathymetry contours

highest resonant frequency Kelvin wave for insight as to why it was not observed. In addition, we consider the "non-oscillatory" Kelvin wave where the forcing is turned on at the beginning of the simulation and then held constant (i.e., a step function wave). This non-oscillatory signal is considered to gain insight into the propagation of signals arising from sustained changes in coastal Antarctic winds, and is most consistent with the experiments of Spence et al. (2017) and Webb et al. (2019). While this Kelvin wave will be denoted by the frequency label ω_0, and referred to as having a frequency of "0," it is important to note that such a step function actually contains contributions from all frequencies. However, as most of our analysis is based on averages over a week or a month of simulation, in practice, the ω_0 results are dominated by the lowest frequencies.

In the series of eastern-boundary-forced experiments, in order to isolate the amount of scattering of Kelvin waves into Rossby waves, we adjust the parameters f and H to be either constant or variable. The Coriolis parameter, f, is fixed to its value at 60°S for cases where rotation is kept constant and an average depth of 4000m is assumed for cases where H is constant. In the case of variable depth, etopo5 bathymetry (Data Announcement 88-MGG-02 1988) is used at 1° resolution. To estimate the amount of scattering due to Drake Passage jumping, the global model described above is used both with and without landmasses north of 60°S and compared for cases both with and without variations in f and H.

4 Results

Here we analyze the energetics of barotropic Kelvin wave propagation around Antarctica. We begin with the simplest single-layer case where only the coastal geometry for Antarctica is present with f and H held constant. We then systematically introduce increasing complexity, adding coastal geometry north of Antarctica, turning on variations in f and H, and testing the sensitivity to forcing conditions.

4.1 Coastal geometry

Comparing the energy flux of the propagating Kelvin wave at different locations around Antarctica in the case with only coastal geometry variations (Fig. 2.) shows that, as expected, no energy is lost to Poincaré waves below the inertial frequency ($\omega < f_0$, i.e., for ω_1 and ω_2). For the ω_0 step-function forcing a similar result holds — with the loss of energy from the super-inertial components of the step function occurring only as a brief transient as the initial wave-front passes. For the super-inertial frequencies ω_3 and ω_4, we find that the energy flux drops by approximately 80% and 90% respectively over one propagation cycle around Antarctica with non-re-entrant boundary conditions (results from these non-re-entrant boundary condition simulations are summarized in Table 1). Thus, the majority of high-frequency coastal Kelvin wave energy is scattered away from the Antarctic coastline due to changes in coastal geometry alone. The largest drop in energy for the ω_3 frequency is seen between Drake Passage and New Zealand, corresponding to 20% of the initial Kelvin wave energy flux going into the Pacific Ocean (Fig. 3a). The change in energy flux is most prominent in this region due to the number of sharp coastal angles at large scales, such as the West Antarctic Peninsula and Ross Sea embayment. As the frequency increases, we find the propagating Kelvin wave to be more sensitive to smaller scale features in the coastline (i.e., sensitivity increases as the wavelength becomes comparable to the spatial scale of more coastal

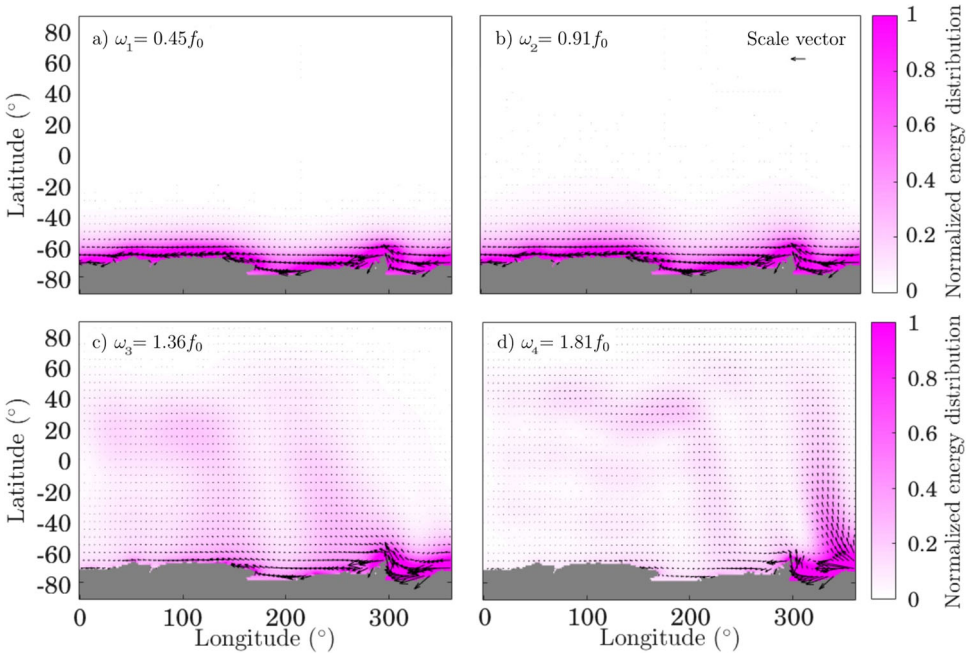

Fig. 2 Barotropic eastern-boundary-forced normalized energy distribution (dimensionless), wave-period averaged within the first month for (a–b) sub-inertial ($\omega < f_0$) and (c–d) super-inertial ($\omega > f_0$) Kelvin waves with constant Coriolis parameter (evaluated at 60°S, i.e., $f_0 = 1.26 \times 10^{-4} s^{-1}$), constant depth (4000m), and no landmass above 60°S. Black arrows indicate the energy flux vectors. The scale vector (b) indicates the size of the energy flux on the coast on the eastern boundary. The energy distribution is normalized by the average energy within one deformation radius away from the Antarctic coastline along the eastern boundary

features). That is, for the ω_4 frequency, the initial Kelvin wave loses 60% of its energy before reaching Drake Passage, with approximately 35% passing into the Atlantic.

4.2 Drake passage

When coastal landmasses are included north of 60°S with constant Coriolis parameter and depth (4000m), we find that all oscillatory Kelvin wave frequencies (i.e., $\omega \neq 0$) lose 10–20% of their energy passing through Drake Passage (Figs. 3b and 4). The energy loss is consistent across these frequencies as the deformation radius does not depend on frequency. This energy loss corresponds to energy (flux) gain in the Atlantic of 10–20% for ω_1, ω_2, and ω_3, and 55% for ω_4 (the larger energy loss for this frequency being caused by coastal geometry as discussed in Section 4.1). At time-scales less than approximately 1 month from initial forcing, the differences between the loss of energy flux through Drake Passage and the energy gain into the Atlantic is due to the build of energy ($\partial E/\partial t$) in the Atlantic sector of the Southern Ocean (between 90–30 ° S and 290–360 ° E; indicated by blue lines in Fig. 3), with dissipation due to bottom drag being negligible for the chosen bottom drag coefficient. Over time-scales longer than this, we see an equilibration between the energy flux through Drake Passage and the energy flux into the Atlantic. However, these longer time-scale energy fluxes are affected by the return of waves from the Northern Hemisphere back southwards, which is unrealistic here as f is constant. Thus, in order to isolate the amount of Kelvin wave energy crossing Drake Passage in one propagation cycle, we focus on the short time-scale response (i.e., within the first month) for the rest of the eastern boundary forced cases.

For the non-oscillatory case (ω_0), we find approximately 99% of the energy remains along the Antarctic coastline during its propagation cycle with only 1% of its initial

Table 1 Summary table for all eastern-boundary-forced oscillatory cases, indicating model configuration (first four columns) and energy transmission (ingoing energy flux/outgoing energy flux; last four columns) of Kelvin waves in one propagation cycle around Antarctica, wave-period averaged within the first month of simulation

Antarctic coast	Land mass > 60°S	Varying f	Varying H	$\lvert\mathbf{F}_{out}\rvert/\lvert\mathbf{F}_{in}\rvert$				
				ω_0	ω_1	ω_2	ω_3	ω_4
No	No	No	No	1	1	1	1	1
Yes	No	No	No	1	1	1	0.21	0.08
Yes	Yes	No	No	0.99	0.89	0.84	0.22	0.04
Yes	Yes	Yes	No	0.98	0.58	0.41	0.09	0.04
Yes	Yes	No	Yes	0.08	0.24	0.41	0.04	0.01
Yes	Yes	Yes	Yes	0.07	0.28	0.26	0.04	0.01

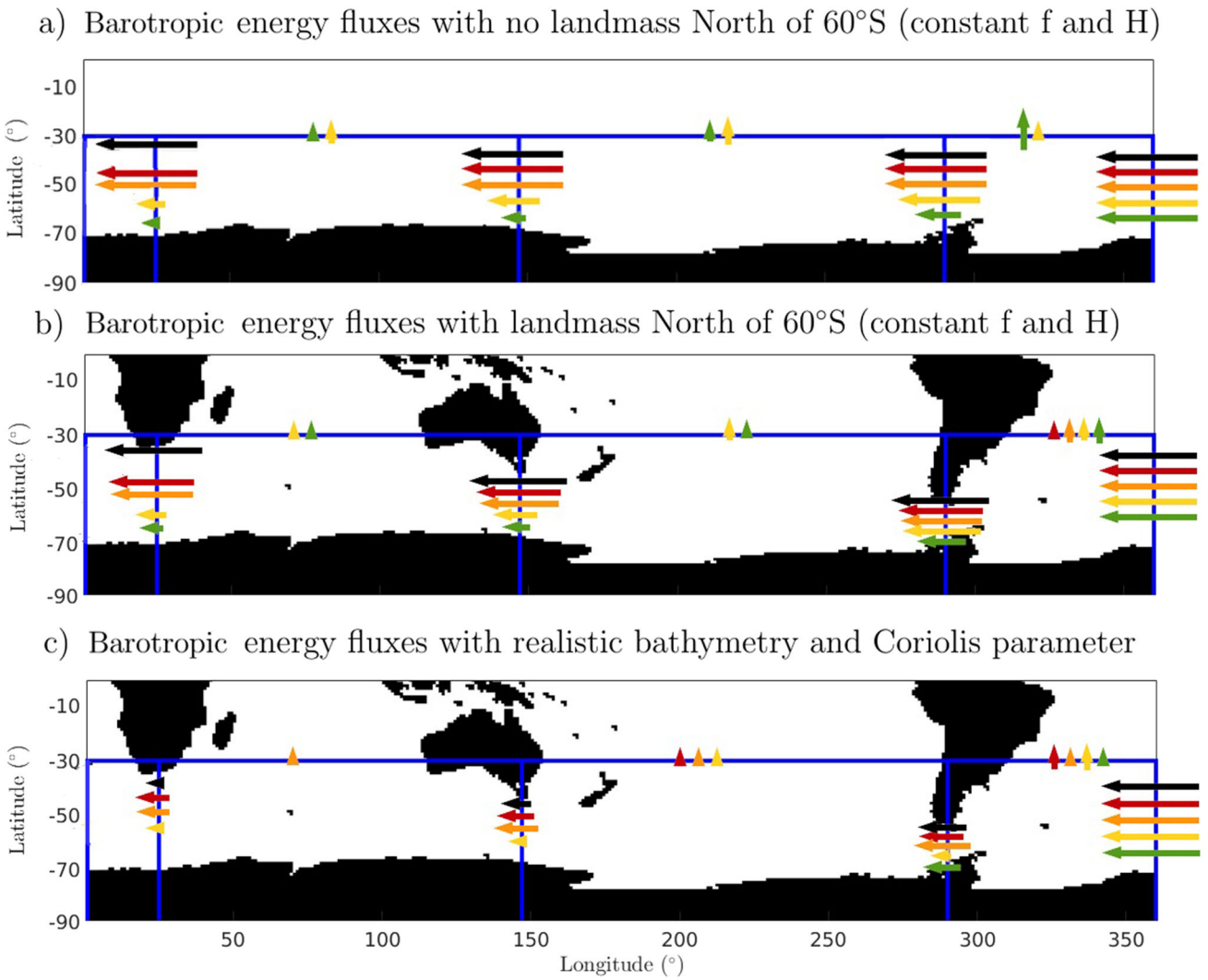

Fig. 3 Barotropic eastern-boundary-forced normalized energy fluxes (dimensionless), wave-period averaged within the first week of initialization for sub-inertial (ω_0 — black, ω_1 — red, and ω_2 — orange arrows) and super-inertial (ω_3 — yellow and ω_4 — green arrows) Kelvin waves around Antarctica. Energy fluxes are calculated in the non-reentrant boundary experiments for (a) constant Coriolis parameter, constant depth (4000m), and no landmass above 60°S; (b) constant Coriolis parameter and constant depth (4000m); and (c) both realistic bathymetry and Coriolis parameter. Blue lines indicate the line segments where the energy fluxes are summed over. Normalized energy fluxes with magnitude less than 2% of the initially forced Kelvin wave are not shown

energy flux entering the North Atlantic (Fig. 3a, red line in Figs. 4 and 5a). To better understand the difference between non-oscillatory and oscillatory waves, we tested a range of frequencies between 0 and ω_1 and find that there is a gradual transition between the non-oscillatory result of no Drake Passage jumping and the higher frequencies where increasing amounts of energy penetrate into the North Atlantic (Fig. 6). Non-oscillatory (steady) waves are not able to cross Drake Passage as a time-mean zonal pressure gradient cannot be sustained across Drake Passage. As frequency increases, transient zonal pressure gradients are permitted, allowing northward propagation across Drake Passage.

4.3 Bathymetry and coriolis

Comparing cases with both realistic Coriolis parameter and bathymetry, we find that the sub-inertial frequencies lose approximately 75% of their initial energy in one propagation cycle. Kelvin wave interactions with bathymetry generate topographic waves that propagate away from Antarctica, reducing Kelvin wave energy in almost every location along the Antarctic coastline at all frequencies (shown for ω_0, ω_1, and ω_3 in Figs. 5, 7, and 8 respectively). Super-inertial frequency Kelvin waves are found to lose more than 95% of their energy in one cycle due to a combination of interactions with bathymetry and coastal geometry (Fig. 8). The

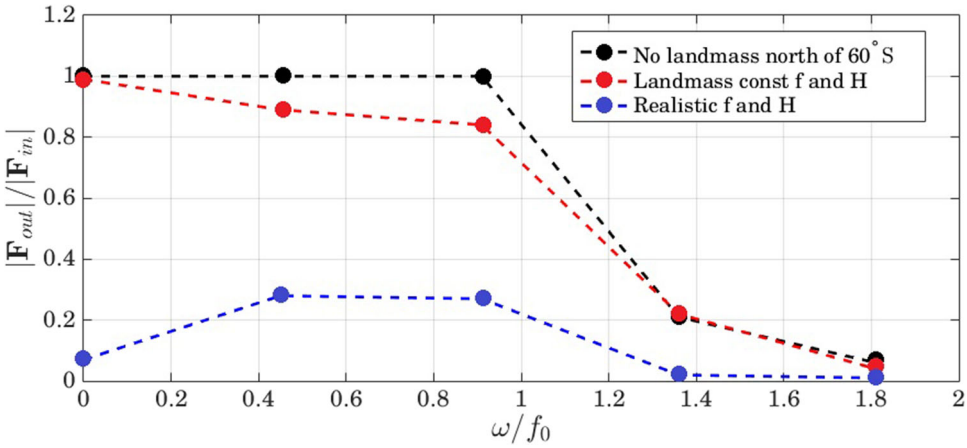

Fig. 4 Energy flux ratios of outgoing (0°E) to ingoing (360°E) barotropic Kelvin waves in one cycle around Antarctica (forced from the eastern boundary), wave-period averaged within the first month. Energy flux ratios are shown for: no landmass North of 60°S (black), constant depth and Coriolis parameter (red), and realistic bathymetry and Coriolis parameter (blue)

majority of energy loss for high-frequency Kelvin waves occurs before reaching New Zealand - these waves cannot sustain a consistent signal around Antarctica. This confirms that long time-scale build up of energy due to barotropic Kelvin wave propagation around Antarctica (e.g., Spence et al. 2017) will be dominated by the low-frequency modes.

When re-entrant boundary conditions are added, we find similar energy losses around Antarctica in one-cycle for each forcing scenario within the first week. Since energy can no longer radiate out of the western boundary, and the frequencies we have chosen are resonant around Antarctica, we also see a stronger energy build-up over time (Fig. 9). Sea surface height anomalies gradually build with each cycle of the Kelvin wave propagating around Antarctica. However, when the energy distribution is normalized to the forcing region (i.e., by dividing each value by the wave-period averaged energy density in the forcing region), the results remain consistent with the eastern boundary forcing cases.

Interestingly, we see different spatial distributions of energy density in the wind-forced experiments depending on the temporal frequency of the wind forcing, even between different sub-inertial frequencies and between different super-inertial frequencies (Fig. 9). For example,

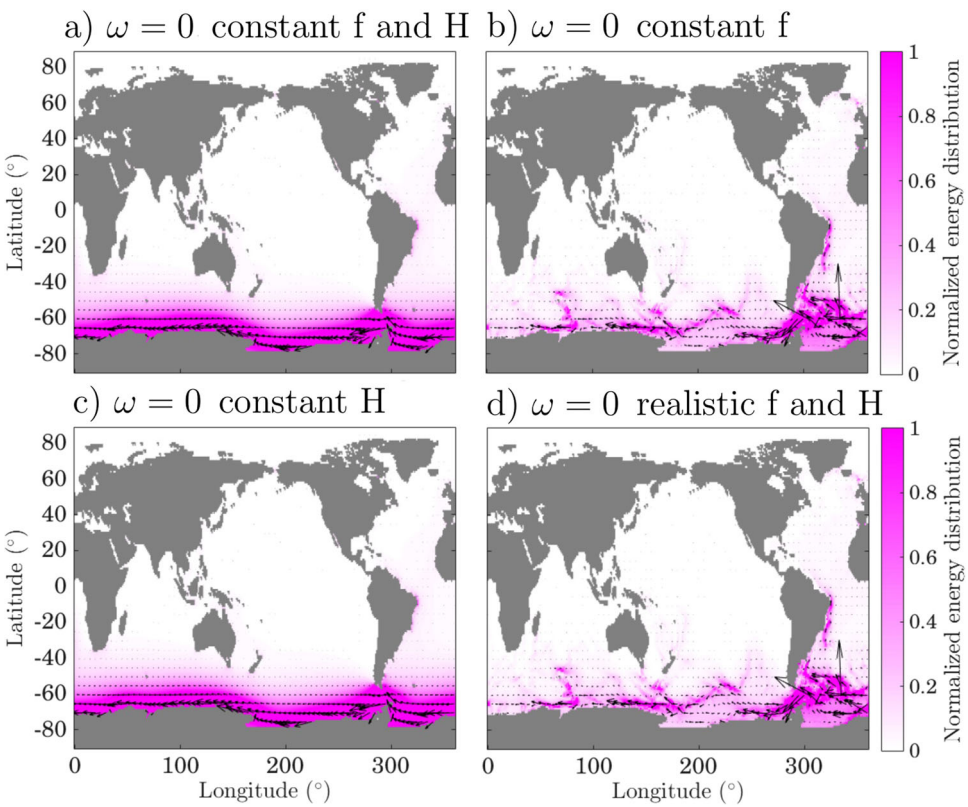

Fig. 5 Energy distribution of eastern-boundary-forced non-oscillatory barotropic Kelvin waves (ω_0) around Antarctica for (a) constant depth and Coriolis parameter, (b) realistic bathymetry and constant Coriolis parameter, (c) constant depth and realistic Coriolis parameter, and (d) both realistic bathymetry and Coriolis parameter, wave-period averaged within the first week. Energy distribution is normalized to the Kelvin wave signal in the forcing region and black arrows indicate the normalized energy flux vectors

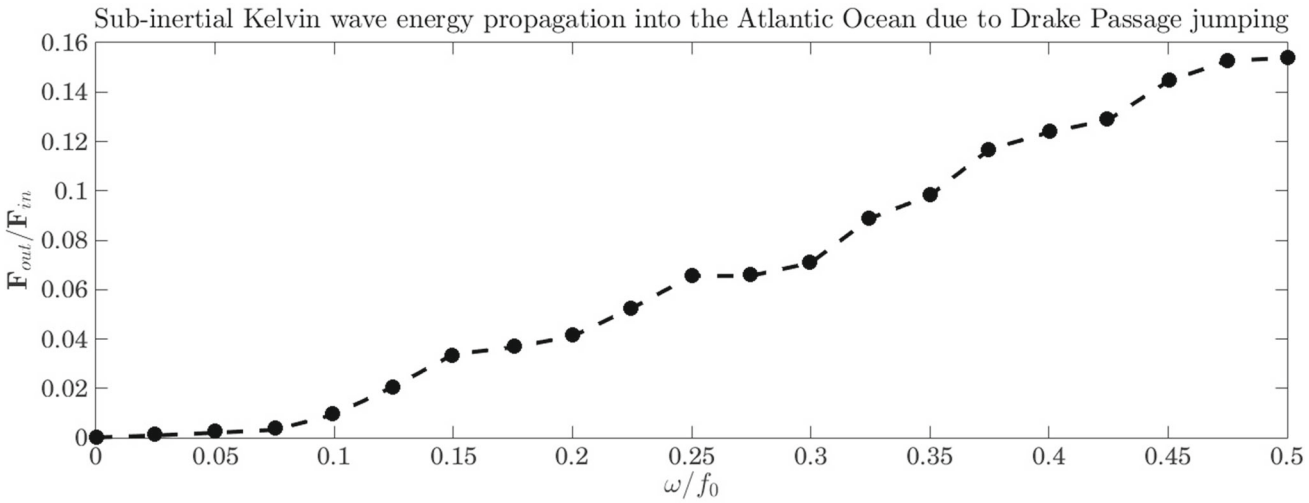

Fig. 6 Energy flux ratios of eastern-boundary-forced low-frequency barotropic Kelvin waves from the forcing region (90°S − 30°S; 360°E) to the energy propagating into the Atlantic Ocean (30°S; 290°E − 360°E; shown by blue lines in Fig. 2) within 1 week of initialization. Energy flux ratios are shown for the case with realistic bathymetry and Coriolis parameter

the ω_1 frequency has a large signal in the North Atlantic and is nearly non-existent in the Indo-Pacific region (Fig. 9a). The situation is reversed for the ω_2 frequency (Fig. 9b). We suspect these differences are partially caused by the ability of waves with smaller wavelengths to penetrate into smaller channel widths. In general, we find sub-inertial frequencies appear to have more influence on coastal regions around the globe, while super-inertial frequencies appear to propagate their energy into the open ocean. This is consistent with our findings of super-inertial Kelvin waves losing their energy to Poincaré waves along significant portions of the Antarctic coastline.

We also tested the sensitivity of these results to the location of the wind forcing, by shifting the forcing region to 145°E–245°E (Fig. 10). Overall, the energy loss from a complete cycle around Antarctica is consistent with

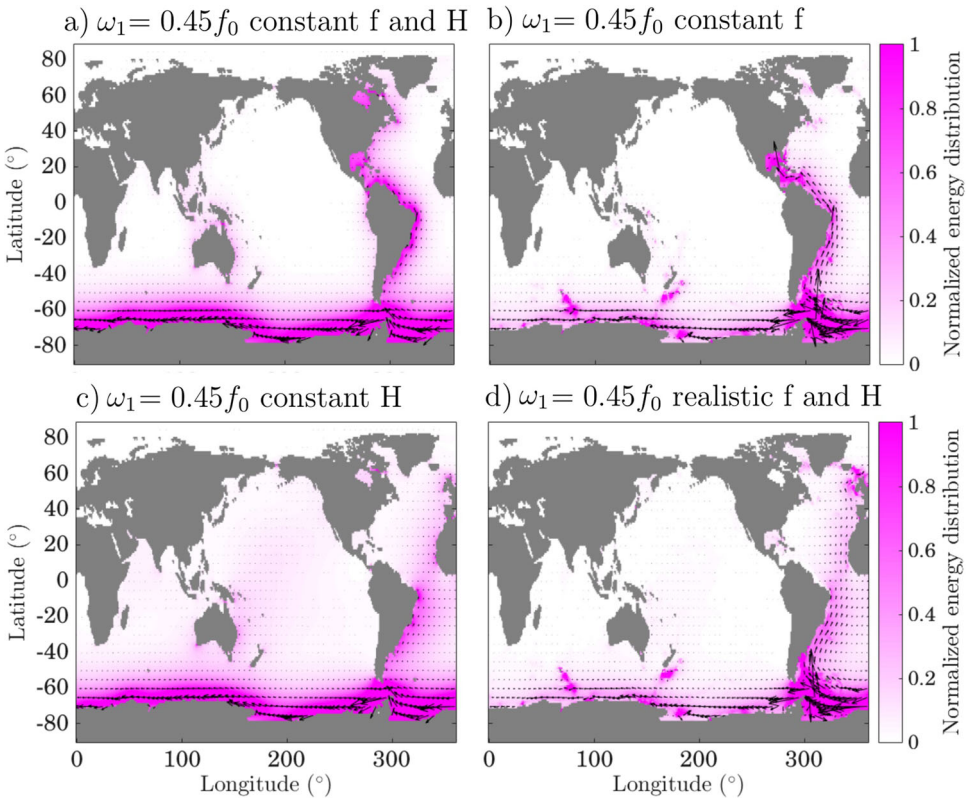

Fig. 7 Energy distribution of eastern-boundary-forced sub-inertial barotropic Kelvin waves (ω_1) around Antarctica for (a) constant depth and Coriolis parameter, (b) realistic bathymetry and constant Coriolis parameter, (c) constant depth and realistic Coriolis parameter, and (d) both realistic bathymetry and Coriolis parameter within 1 week. Energy distribution is normalized to the Kelvin wave signal in the forcing region (i.e., by dividing all values by the wave-period averaged energy density within the deformation radius along the eastern boundary) and black arrows indicate the normalized energy flux vectors

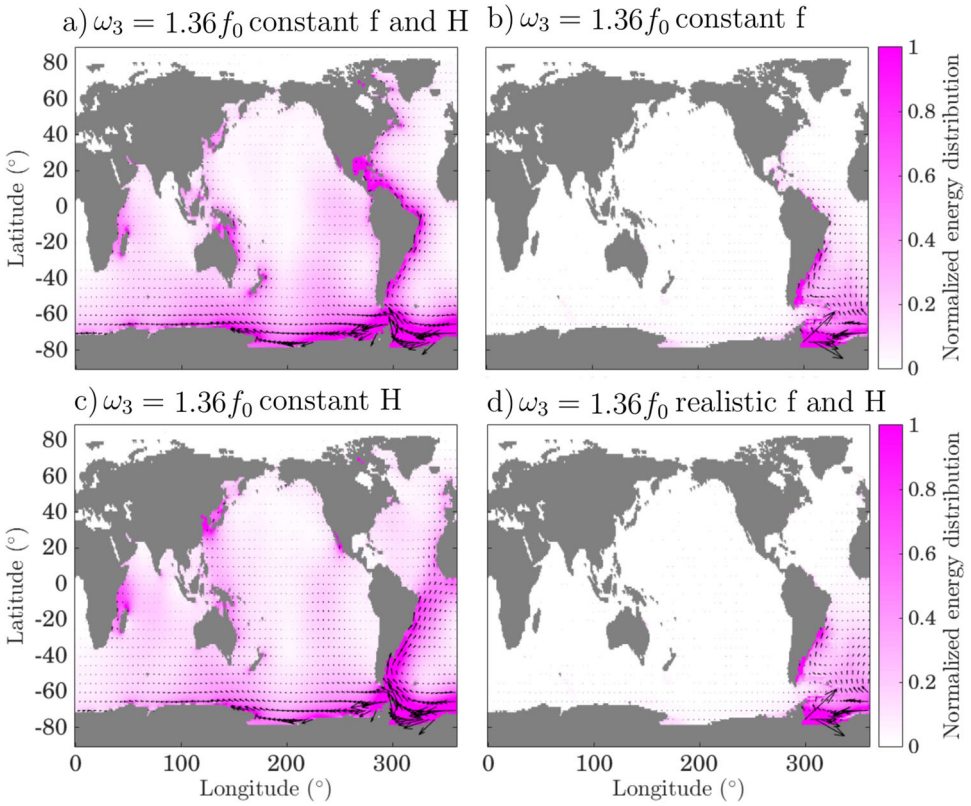

Fig. 8 Energy distribution of eastern-boundary-forced super-inertial barotropic Kelvin waves (ω_3) around Antarctica for (a) constant depth and Coriolis parameter, (b) realistic bathymetry and constant Coriolis parameter, (c) constant depth and realistic Coriolis parameter, and (d) both realistic bathymetry and Coriolis parameter, wave-period averaged within first week . Energy distribution is normalized to the Kelvin wave signal in the forcing region and black arrows indicate the normalized energy flux vectors

the 20°E–120°E location for all frequencies. However, the location of the energy loss differs depending on the frequency. The energy distributions for both ω_1 and ω_2 remain relatively consistent between wind-forcing scenarios. The main difference being a larger energy density for ω_2, particularly in and westward of the forcing region (Fig. 10b). This is consistent with the fact that scattering of sub-inertial frequencies is dominated by bathymetry. There are no major bathymetric features in East Antarctica until Drake Passage, where the ω_1 and ω_2 signals are scattered away from the Antarctic coastline, resulting in a significant reduction in energy density directly west of Drake Passage (Fig. 10a–b). In contrast, ω_3 and ω_4 energy densities are much larger in the Pacific Ocean, with a weaker signal along the coast when the forcing region is located between 145°E and 245°E (compare Fig. 10c, d with Fig. 9c, d). This is consistent with the prominent scattering of super-inertial waves away from the coast through changes in coastal geometry. In particular, the ω_3 and ω_4 waves are strongly scattered outward into Poincaré waves by the prominent coastal geometric features surrounding the Ross Sea (Fig. 10c–d). The energy distribution in the ω_0 case is shifted eastward along with the forcing region (compare Figs. 9e and 10e) but otherwise exhibits similar features. Importantly, there is still a significant signal along the West Antarctic Peninsula for the ω_0 case when the forcing region is shifted eastward, despite the signal directly west of the forcing region being weaker. This may be a consequence of barotropic flow converging over the steep topography on the West Antarctic Peninsula where f/H contours are closely spaced (Hughes et al. 1999; Langlais et al. 2015; Spence et al. 2017; Webb et al. 2019).

5 Discussion and conclusions

Barotropic Kelvin waves propagating around the Antarctic continent are thought to play an important role in driving teleconnections between high-latitude and mid/low-latitude climate (e.g., Atkinson et al. 2009), and have been recently implicated in processes leading to warming of the Antarctic continental shelf with implications for Antarctic ice sheet mass loss (Spence et al. 2017; Webb et al. 2019). In order to understand sinks of barotropic Kelvin wave energy around Antarctica, we have studied barotropic Kelvin wave propagation in a suite of idealized model simulations. Using a linear single-layer shallow water model, we systematically introduced variations in coastal geometry, bathymetry, and rotation to evaluate their impact on barotropic Kelvin wave scattering. Two model configurations were used. The first utilized non-reentrant boundary conditions and eastern boundary forcing to examine energy losses during

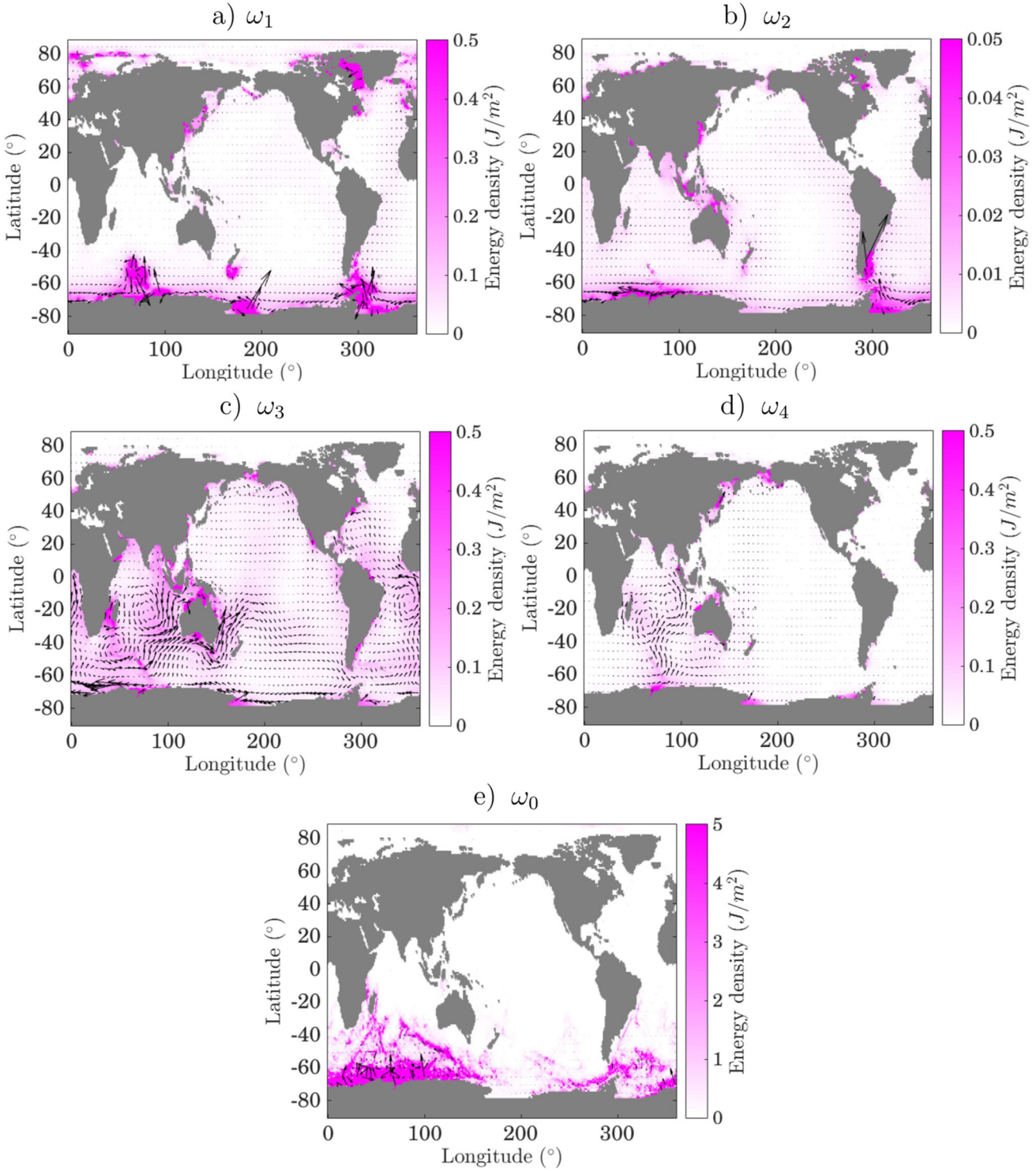

Fig. 9 First month energy densities (J/m^2) of wind forced Kelvin waves around Antarctica for (a) ω_1, (b) ω_2, (c) ω_3, (d) ω_4, and (e) ω_0 frequency Kelvin waves. Idealized oscillating wind anomalies are applied approximately between $20°E$ and $120°E$ (see Fig. 1) with frequencies corresponding to the generated Kelvin wave frequency. Black arrows indicate the normalized energy flux vectors. Different color-axis scales are used for (b) and (e) where relatively weak and strong signals are seen respectively

a single circumnavigation of Antarctica. The second utilized reentrant boundary conditions and was forced with sinusoidal wind stress anomalies (see Fig. 1).

We find the major influence on barotropic Kelvin wave propagation around Antarctica are interactions with topography and coastal geometry, resulting in scattering of

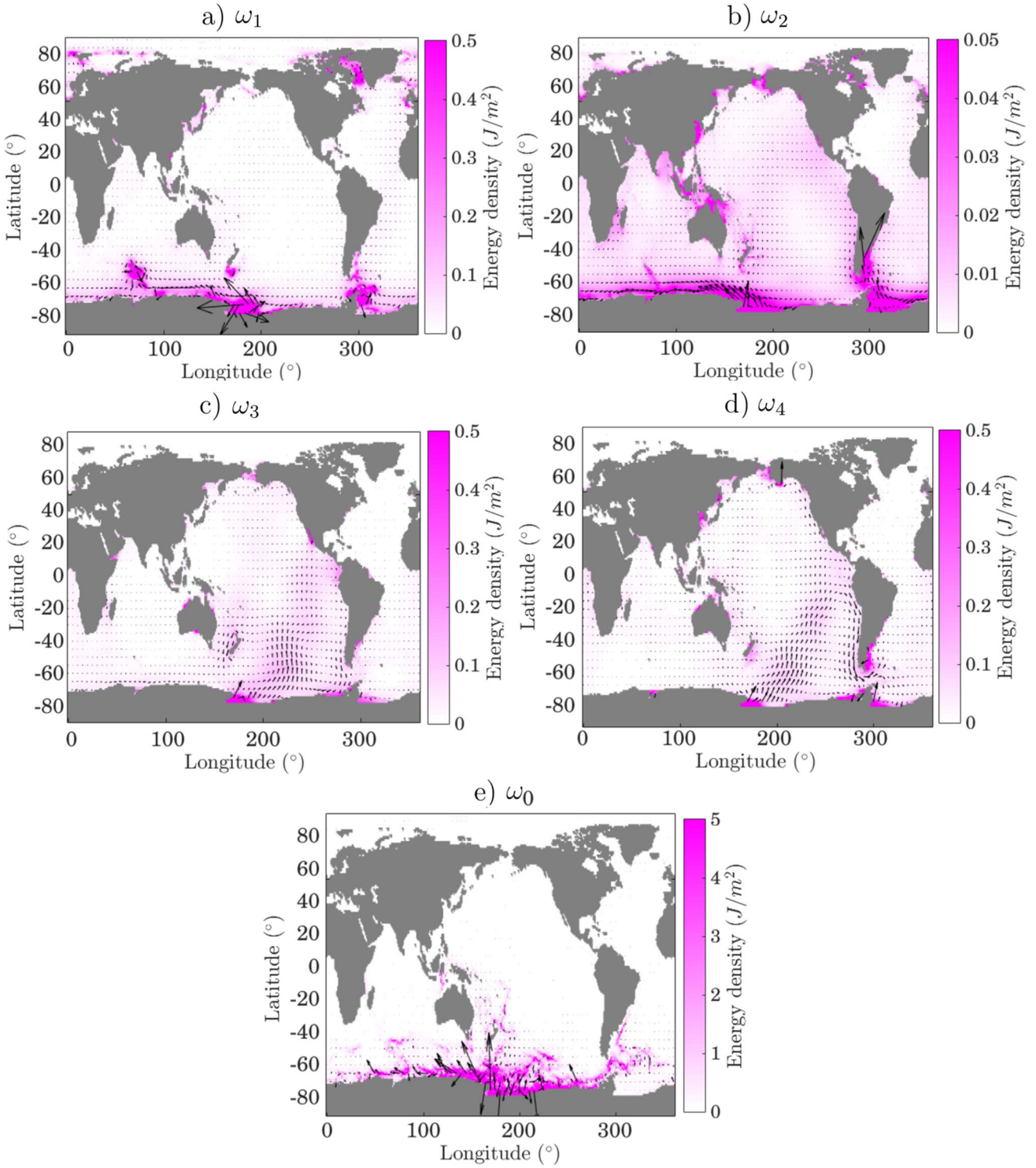

Fig. 10 First month energy densities (J/m^2) of wind forced Kelvin waves around Antarctica for (a) ω_1, (b) ω_2, (c) ω_3, (d) ω_4, and (e) ω_0 frequency Kelvin waves. Idealized oscillating wind anomalies are applied approximately between 145°E and 245°E with frequencies corresponding to the generated Kelvin wave frequency. Black arrows indicate the normalized energy flux vectors. Different color-axis scales are used for (b) and (e) to remain consistent with Fig. 9

Kelvin wave energy to a variety of wave types, including topographic Rossby waves and Poincaré waves. These scattering processes are most pronounced near the Ross Sea and Drake Passage. The behavior of sub-inertial and super-inertial frequencies differs significantly, with up to 75% of sub-inertial barotropic Kelvin wave energy around

Antarctica scattering away from the coast, and up to 95% for super-inertial frequencies, in a single circumnavigation of Antarctica. This difference is attributable to the ability of variations in coastal geometry to scatter Kelvin wave energy into Poincaré waves, which propagate into the open ocean, at super-inertial frequencies but not at sub-inertial frequencies. As a consequence, we also find greater amounts of wave energy accumulates in the open ocean at super-inertial frequencies. Conversely, changes in coastal geometry play little role in the dissipation of sub-inertial Kelvin wave energy along Antarctica (except for allowing transmission across Drake Passage) and we find greater amounts of energy density to accumulate in coastal regions. Instead, interactions with bathymetry lead to the largest sink of energy along the coast at sub-inertial frequencies.

In the wind forced, reentrant boundary conditions scenario, we find the biggest drop in circumpolar Kelvin wave energy flux to be near Drake Passage where there is a combination of scattering by bathymetry and a partial propagation of the signal across Drake Passage, from where it continues northward along the east coast of South America. Thus, over longer time-scales, we suspect only sub-inertial Kelvin waves are able to develop a sizable circumpolar signal. This is enabled by two factors: (1) the incomplete scattering of these waves away from the Antarctic coastline in one cycle (as mentioned above), and (2) the conditions of resonant forcing (Platzman et al. 1981; Kusahara and Ohshima 2014). At these frequencies, the barotropic signal propagates around Antarctica arriving back to the forcing region (albeit as a small percentage of the original signal) where it is then amplified by resonant forcing. For super-inertial frequencies, near complete scattering of Kelvin waves away from Antarctica occurs in a single circumnavigation with ω_3 experiencing the least amount of scattering among super-inertial frequencies. This is consistent with observations, where the ω_1, ω_2, and ω_3 Kelvin waves have been observed around Antarctica, with ω_3 being the weakest signal (Kusahara and Ohshima 2014). However, we note that uncertain bottom dissipation processes may also impact these results. Ponte and Hirose (2004) suggested that dissipation may make global barotropic Kelvin wave signals difficult to observe in reality. While we found no sensitivity to the quadratic bottom drag coefficient included in our model simulations for values between 0 and 1×10^{-3}, this parameter is uncertain and choice of a larger drag coefficient would result in attenuation of the Kelvin wave signal and thus reduced circumpolar propagation. We note that barotropic waves remain prominent in global ocean models where dissipation may be poorly represented and relatively high friction is needed for numerical stability (e.g., Jochum et al. 2008; Spence et al. 2012). These numerical considerations, including the impact of resolution and bottom drag (Killworth 1988; 1989; Griffiths 2013), may become more important when considering the Kelvin wave energetics over longer time-scales.

An additional factor that has not been considered in this article is conversion from barotropic to baroclinic modes. While there is a large scale separation between barotropic and baroclinic waves, previous studies have highlighted the potential for such conversions. For example, Spence et al. (2017) showed indications of barotropic to baroclinic energy conversion on the West Antarctic Peninsula in a general circulation model. Carter et al. (2008) also demonstrate the prominence of barotropic to baroclinic conversion for barotropic tides propagating over a ridge, using high-resolution model simulations. As part of this study, we did perform a number of two-layer shallow water experiments, which showed evidence of some conversion from barotropic to baroclinic modes. However, the behavior of the baroclinic modes is more uncertain given their much stronger interactions with mean flows, background stratification variations, and small-scale features. Thus, we leave a more detailed investigation of barotropic to baroclinic conversion to a future study.

Finally, another point of interest highlighted by this study is the ability for barotropic Kelvin waves to propagate across Drake Passage, leading to teleconnections between Antarctica and the global ocean. Teleconnections from the Southern Ocean to the equatorial region through barotropic Kelvin waves have been highlighted in previous studies (e.g., Ivchenko et al. 2004; Atkinson et al. 2009; Blaker et al. 2006). Here, we found that approximately 10–20% of low-frequency Antarctic barotropic Kelvin wave energy from the East Antarctic forcing region is transported into the Atlantic Ocean. This teleconnection can occur within a few days, due to the rapid propagation speed of barotropic waves, and could potentially alter coastal circulation along eastern regions of South America via the coastal propagation of these waves. Furthermore, the barotropic wave signal can propagate eastward once it has reached the Equator (as an equatorial Kelvin wave) and continue propagating northward (as a coastal Kelvin wave) once it has reached the west coast of Africa, potentially impacting regions in the North Atlantic. Similar propagation mechanisms have been highlighted for baroclinic waves in experiments linking Southern Hemisphere winds to the North Atlantic overturning circulation (McDermott 1996; Brix and Gerdes 2003). Although we find links between Antarctic Kelvin waves and the global ocean, we also see substantial differences in the global barotropic energy density depending on the frequency of the initially forced Kelvin wave. For example, the sub-inertial frequency $\omega_1 = 0.45\, f_0$ wave transports a relatively large energy signal into the North Atlantic region and a negligibly small energy signal into the Indo-Pacific region, whereas the converse

is true for $\omega_2 = 0.91 f_0$. The ability for Kelvin waves to cross Drake Passage also suggests that, apart from local storm systems, Kelvin waves around Antarctica can also be generated from remote locations north of the Drake Passage gap. A sustained Kelvin wave signal around Antarctica can then only develop if it is resonant with the Antarctic circumference, consistent with observations of Kusahara and Ohshima (2014).

Acknowledgements We thank R. Greatbatch and three anonymous reviewers for useful comments. Numerical simulations were conducted at the NCI National Facility systems at the Australian National University through the National Computational Merit Allocation Scheme supported by the Australian Government.

Funding Open Access funding enabled and organized by CAUL and its Member Institutions. This work was supported by the Australian Research Council, including the ARC Centre of Excellence for Climate System Science (CE110001028) the ARC Centre of Excellence for Climate Extremes (CE170100023), the ARC Centre for Excellence in Antarctic Science (SR200100008), and ARC grants FT190100413 (PS) and DE21010004 (RMH). MHE is also supported by the Centre for Southern Hemisphere Oceans Research (CSHOR), a joint research centre between QNLM, CSIRO, UNSW, and UTAS.

Data availability The datasets generated during and/or analyzed during the current study are available from the authors on reasonable request.

Declarations

Conflict of interest The authors declare no competing interests.

References

Atkinson CP, Wells NC, Blaker AT, Sinha B, Ivchenko VO (2009) Rapid ocean wave teleconnections linking Antarctic salinity anomalies to the equatorial ocean-atmosphere system. Geophys Res Lett 36:L08603. https://doi.org/10.1029/ 2008GL036976

Brink KH (1991) Coastal-trapped waves and wind-driven currents over the continental shelf. Annu Rev Fluid Mech 23:389–412

Brix H, Gerdes R (2003) North atlantic deep water and antarctic bottom water: their interaction and influence on the variability of the global ocean circulation. J Geophys Res, 108. https://doi.org/10.1029/2002JC001

Blaker AT, Sinha B, Ivchenko VO, Wells NC, Zalesny VB (2006) Identifying the roles of the ocean and atmosphere in creating a rapid equatorial response to a Southern Ocean anomaly. Geophys Res Lett 2006:33. https://doi.org/10.1029/2005GL025474

Buchwald V, Miles J (1974) Kelvin-wave diffraction by a gap. J Aust Math Soc 17(1):29–34. https://doi.org/10.1017/S1446788700015925

Carter GS, Merrifield MA, Becker JM, Katsumata K, Gregg MC, Luther DS, Levine MD, Boyd TJ, Firing YL (2008) Energetics of M2 barotropic-to-baroclinic tidal conversion at the Hawaiian Islands. J Phys Oceanogr 38:2205–2223. https://doi.org/10.1175/2008JPO3860.1

Chapman DC (1985) Numerical treatment of cross-shelf open boundaries in a barotropic coastal ocean model. J Phys Oceanogr 15:1060–1075. https://doi.org/10.1175/1520-0485(1985)015<1060:NTOCSO>2.0.CO;2

Data Announcement 88-MGG-02 (1988) Digital relief of the surface of the Earth. NOAA, national geophysical data center. Boulder, Colorado

Flather RA (1976) A tidal model of the northwest European continental shelf. Memoires de la Societe Royale de Sciences de Liege 6:141–164

Fu LL, Keffer T, Niiler PP, Wunsch C (1982) Observations of mesoscale variability in the western North Atlantic; a comparative study. J Mar Res 40:809–848

Garrett C (1978) Topographic Rossby waves off east australia: Identification and role in shelf circulation. J Phys Oceanogr 9:244–253

Griffiths SD (2013) Kelvin wave propagation along straight boundaries in C-grid finite-difference models. J Comp Sci 255:639–659. https://doi.org/10.1016/j.jcp.2013.08.040

Hughes CW, Meredith MP, Heywood KJ (1999) Wind-Driven Transport fluctuations through drake passage: a southern mode. J Phys Oceanogr 29(8):1971–1992

Huthnance JM (1978) On coastal trapped waves: analysis and numerical calculation by inverse iteration. J Phys Oceanogr 8:74–92

Huthnance JM (1980) Waves and currents near the continental shelf edge. Prog Oceanogr 10(4):193–226. https://doi.org/10.1016/0079-6611(81)90004-5

Ivchenko VO, Zalesny VB, Drinkwater MR (2004) Can the equatorial ocean quickly respond to Antarctic sea ice/salinity anomalies? Geophys Res Lett, 31

Jayne SR, Marotzke J (2001) The dynamics of wind-induced ocean heat transport variability. Rev Geophys 39:385–411

Jochum M, Danabasoglu G, Holland M, Kwon Y-O, Large WG (2008) Ocean viscosity and climate. J Geophys Res 113:C06017. https://doi.org/10.1029/2007JC004515

Johnson HL, Marshall DP (2002) A theory for the surface Atlantic response to thermohaline variability. J Phys Oceanogr 32:1121–1132. https://doi.org/10.1175/1520-0485(2002)032,1121:ATFTSA.2.0.CO;2

Killworth PD (1988) How much of a baroclinic coastal Kelvin wave gets over a ridge? J Phys Ocean 19:321–341

Killworth PD (1989) Transmission of a two-layer coastal Kelvin wave over a ridge. J Phys Ocean 19:1131–1148

Kusahara K, Ohshima KI (2014) Kelvin waves around antarctica. J Phys Ocean 44:2909–2920

LaCasce JH (2017) The prevalence of oceanic surface modes. Geophys Res Lett 44:11,097–11,105. https://doi.org/10.1002/2017GL075430

Langlais CE, Rintoul SR, Zika JD (2015) Sensitivity of Antarctic Circumpolar Current transport and eddy activity to wind patterns in the Southern Ocean. J Phys Oceanogr 45:1051–1067. https://doi.org/10.1175/JPO-D-14-0053.1

Lianillo R (2013) Using a resolution function to regulate parameterizations of oceanic mesoscale eddy fields. Ocean Modeling 72:92–103

Mysak LA (1980) Topographically trapped waves. Ann. Rev. Fluid Mech 12:45–76

Mercer D, Sheng J, Greatbatch RJ, Bobanović J (2002) Barotropic waves generated by storms moving rapidly over shallow water. J. Geophys. Res. 107(C10):3152. https://doi.org/10.1029/2001JC001140

McDermott DA (1996) The regulation of northern overturning by Southern Hemisphere winds. J Phys Oceanogr 26:1234–1255. https://doi.org/10.1175/1520-0485(1996)026,1234:TRONOB.2.0.CO;2

McKee DC, Martinson DG (2020) Wind-driven barotropic velocity dynamics on an Antarctic shelf. J Geophys Res Oceans 125:e2019JC015771. https://doi.org/10.1029/2019JC015771

Packham BA, Williams WE (1968) Diffraction of Kelvin waves at a sharp bend. J Fluid Mech 34, part 3:517–529

Platzman GW, Curtis GA, Hansen KS, Slater RD (1981) Normal modes of the world ocean. Part II: description of modes in the period range 8 to 80 hours. J Phys Oceanogr 1981(11):579–603

Pickart R (1995) Gulf stream-generated topographic Rossby waves. J Phys Oceanogr 25:574–586

Pietri A, Echevin V, Testor P, Chaigneau A, Mortier L, Grados C, Albert A (2014) Impact of a coastal-trapped wave on the near-coastal circulation of the Peru upwelling system from glider data. J Geophys Res Oceans 119:2109–2120. https://doi.org/10.1002/2013JC009270

Ponte R, Hirose N (2004) Propagating bottom pressure signals around Antarctica at 1-2 day periods and implications for ocean modes. J Phys Oceanograp, 34. https://doi.org/10.1175/1520-0485(2004)034<0284:PBPSAA¿2.0.CO;2

Rhines PB (1969) Slow oscillations in an ocean of varying depth: Part 1. Abrupt topography. J Fluid Mech 37(1):161–189

Rignot E, Vaughan DG, Schmeltz M, Dupont T, MacAyeal D (2002) Acceleration of Pine Island and Thwaites glaciers, West Antarctica. Ann Glaciol 34:189–194. https://doi.org/10.3189/172756402781817950

Rosier SHR, Green JAM, Scourse JD, Winkelmann R (2014) Modeling Antarctic tides in response to ice shelf thinning and retreat. J Geophys Res Oceans 119:87–97

Schmidtko S, Heywood KJ, Thompson AF, Aoki S (2014) Multidecadal warming of Antarctic waters. Science 346:1227–1231. https://doi.org/10.1126/science.1256117

Shchepetkin AF, McWilliams JC (2005) The Regional Ocean Modeling System (ROMS): a split-explicit, free-surface, topography following coordinate ocean model. Ocean Modeling 9:347–404

Simionato CG, Meccia V, Dragani W, Nuñez M (2005) Barotropic tide and baroclinic waves observations in the río de la Plata Estuary. J Geophys Res 110:C06008. https://doi.org/10.1029/2004JC002842

Spence P, Saenko OA, Sijp W, England M (2012) The role of bottom pressure torques on the interior pathways of north atlantic deep water. J Phys Oceanogr 42(1):110–125. https://doi.org/10.1175/2011JPO4584.1

Spence P, Holmes RM, Hogg AM, Griffies SM, Stewart KD, England MH (2017) Localized rapid warming of West Antarctic subsurface waters by remote winds. Nat Clim Chang 7:595–603. https://doi.org/10.1038/nclimate3335

Stewart AL, Klocker A, Menemenlis D (2018) Circum-antarctic shoreward heat transport derived from an eddy- and tide-resolving simulation. Geophys Res Lett 2018(45):834–845. https://doi.org/10.1002/2017GL075677

Taylor GI (1922) Tidal oscillations in gulfs and rectangular basins. Proc Lond Math Soc 1922(s2–20):148–181. https://doi.org/10.1112/plms/s2-20.1.148

Webb DJ, Holmes RM, Spence P, England MH (2019) Barotropic Kelvin wave-induced bottom boundary layer warming along the West Antarctic Peninsula. J Geophys Res Oceans 124:1595–1615. https://doi.org/10.1029/2018JC014227

Webb DJ, Spence P, Holmes RM, England MH (2021) Planetary-wave-induced strengthening of the AMOC forced by poleward intensified southern hemisphere westerly winds. Journal of Climate 34:7073–7090. https://doi.org/10.1175/JCLI-D-20-0858.1

Wilkin JL, Chapman DC (1990) scattering of coastal-trapped waves by irregularities in coastline and topography. J Phys Oceanogr 20:396–421

Zahel W, Müller M (2005) The computation of the free barotropic oscillations of a global ocean model including friction and loading effects. Ocean Dynamics 55:137–161